Slowing down supercooled liquids by manipulating their local structure

Susana Marín-Aguilar, Henricus H Wensink, Giuseppe Foffi, Frank Smallenburg

Soft Matter

Accepted Manuscript

This article can be cited before page numbers have been issued, to do this please use: S. Marín Aguilar, H. H. Wensink, G. Foffi and F. Smallenburg, *Soft Matter*, 2019, DOI: 10.1039/C9SM01746A.

ROYAL SOCIETY OF CHEMISTRY

rsc.li/soft-matter-journal

View Article Online
DOI: 10.1039/C9SM01746A

Soft Matter

ARTICLE TYPE

Cite this: DOI: 00.0000/xxxxxxxxxx

Slowing down supercooled liquids by manipulating their local structure†

Susana Marín-Aguilar,[a] Henricus H. Wensink,[a] Giuseppe Foffi‡[a] and Frank Smallenburg ‡[a]

Received Date
Accepted Date

DOI: 00.0000/xxxxxxxxxx

Glasses remain an elusive and poorly understood state of matter. It is not clear how we can control the macroscopic dynamics of glassy systems by tuning the properties of their microscopic building blocks. In this paper, we propose a simple directional colloidal model that reinforces the optimal icosahedral local structure of binary hard-sphere glasses. We show that this specific symmetry results in a dramatic slowing down of the dynamics. Our results open the door to controlling the dynamics of dense glassy systems by selectively promoting specific local structural environments.

1 Introduction

When we cool down or compress a liquid sufficiently rapidly to avoid crystallization, we end up with a glass: a dynamically arrested state of matter which lacks long-range order. Glasses are ubiquitous in condensed matter and can be found in fields of great technological interest, including materials science, biomaterials, food science, and polymer physics. Although the transition from a fluid into a glass is dramatic from a dynamics perspective, it is accompanied by surprisingly little structural change: structurally, a fluid and a glass can look extremely similar[1–3]. For this reason, the bottom-up design of a glass former is not a trivial task. In order to reliably reach a glassy state via cooling, the dynamics of the system have to slow down rapidly with decreasing temperature, such that the system avoids crystallization. Hence, the question is: how do we design particles with interactions capable of inducing slow dynamics? It is well understood that glassy dynamics are often accompanied by the emergence of long-lived locally favored structures (LFS)[4–12]. In some (but not all) glass formers, these structures have been demonstrated to also correlate directly with local mobility (see e.g. Refs.[3,13]), and hence can be considered at least partially responsible for dynamical slowdown. In order to better understand the microscopic mechanisms behind glass formation, it would be extremely useful to unravel how manipulation of the local structure of a glass former can be used to control its propensity for facilitating dynamical arrest.

Simple fluids consisting of particles with short-ranged isotropic interactions are an extremely convenient playground for exploring the interplay between local structure and dynamics. Two of the most fundamental examples are hard spheres and square-well particles, providing a purely repulsive and an attractive isotropic model system, respectively. In order to avoid crystallization, studies typically use a mixture of two or more sizes of particles. Both hard-sphere and square-well models have been widely studied experimentally, numerically and theoretically for their high-density glassy behavior[14–18]. In particular, short-ranged attractive potentials display a remarkable reentrant glassy behavior[17–24], in which the supercooled liquid first speeds up and then slows down again upon cooling, resulting in a maximum in the diffusivity.

In this work, we add directionality to these model systems by exploring the dynamics of supercooled liquids of particles decorated with attractive patches on their surface, interpolating between the limiting cases of pure hard spheres and square-well particles. Our model is inspired by the growing experimental availability of patchy colloidal particles[25–31]. The ability of these particles to form well-defined directional bonds allows them to self-assemble into open crystal structures[32,33] and (at low densities) into strong network-forming glasses[28,34,35]. More importantly, carefully designed anisotropic interactions intuitively favor different local structures in the fluid, and have been shown to be effective at suppressing crystallization[36–38]. Therefore, as one of the most versatile families of two-body anisotropic interactions, patchy particles are an ideal tool for pinning down the role of local structural motifs in the vitrification of dense glasses.

Our extensive computer simulations demonstrate that directional interactions can be designed to selectively promote the motifs responsible for dynamical arrest. We find that the glassy dynamics of patchy systems are remarkably similar for most patch geometries, but exhibit a dramatic slowdown for a select number of patch geometries which enhance icosahedral order, with 12-

[a] Laboratoire de Physique des Solides, CNRS, Université Paris-Sud, Université Paris-Saclay, 91405 Orsay, France

‡ To whom correspondence should be addressed. E-mail: giuseppe.foffi@u-psud.fr and frank.smallenburg@u-psud.fr

† Electronic Supplementary Information (ESI) available: [details of any supplementary information available should be included here]. See DOI: 10.1039/cXsm00000x/

View Article Online
DOI: 10.1039/C9SM01746A

patch particles as the most extreme example. Moreover, we confirm this strong link between icosahedral local order and slow dynamics in a family of polyhedral particles, which achieve similar patchiness due to effective entropic interactions[39]. In both systems, carefully chosen particle geometries are capable of matching and reinforcing the locally favored icosahedral structure of the fluid, providing an ideal route towards the design of systems which facilitate kinetic arrest. As icosahedral geometries also possess five-fold symmetry, which is known to suppress crystallization[36,40–42], particles which boost icosahedral symmetry are likely to be excellent glass formers.

2 Methods

2.1 Model

To model the patchy interactions, we follow the Kern-Frenkel model[43] and model the particles as hard spheres, decorated with n short ranged attractive patches with an opening angle θ. Here, we study systems with 3 to 20 patches, with the patches uniformly distributed over the surface. Specifically, we focus on geometries where the minimum distance between two patches on the surface is maximized (sometimes referred to as spherical codes)[44]. Although this selection is somewhat arbitrary, it ensures an even coverage of the particle surface with patches, and avoids overlapping patches which could strongly affect the bonding behavior. Note that for 11 and 12 patches, this results in patches placed on the vertices of an icosahedron, where for 11 patches there is one vertex omitted. To have a wider picture of the effect of icosahedral patch placement, we also simulate one alternative geometry for particles with 10 patches, where we follow the geometry of the 12-patch case, but omit two opposite vertices. We refer to this geometry as 10_{ico}. We define the patch coverage fraction χ as the fraction of the surface of a particle which is covered by a patch. As long as the patches do not overlap, $\chi = n(1-\cos\theta)/2$, with n the number of patches. For given choice of n and θ, we obtained a certain surface coverage χ. A representation of various angles as well as most of the patch geometries studied in this article are presented in Fig. 1.

In order to suppress crystallization, we simulate a binary mixture of Kern-Frenkel particles of two sizes, with the size ratio given by $\sigma_S/\sigma_L = 0.833$, where $\sigma_{L(S)}$ denotes the size of the large (small) spheres. Two attractive patches form a bond with bonding energy ε when they overlap. The size of each patch is controlled by an opening angle θ and a fixed maximum interaction range $r_c = 1.031\sigma_{ij}$, where σ_{ij} is the contact distance between particles i and j. This interaction range was chosen to be consistent with the square-well interaction in Ref. 22. We restrict our model to only allow a single bond for any pair of particles, even if multiple patches on the same particle overlap. With this restriction, the model interpolates between the hard-sphere model at $\theta = 0$ and the square-well model when θ is larger than a critical θ_f where the patches cover the entire sphere surface.

2.2 Patchy particle simulations

To simulate the patchy particles, we use event-driven molecular dynamics (EDMD) simulations[34,45] with periodic boundary conditions. In each system, we fix the number of particles $N = 700$, the composition $x = 0.5$, and the packing fraction $\eta = 0.58$. At this packing fraction, the square-well limit of our system displays a clear reentrance in the dynamics as a function of temperature[22]. The systems were equilibrated at fixed temperature for at least $10^4\tau$, where $\tau = \sqrt{m\sigma_L^2/k_BT}$ is our time unit, T is the temperature, m is the mass of a particle and k_B is Boltzmann's constant. We then analyze the structure and dynamics of the system in simulations at fixed energy. Note that we report all dynamical quantities for the large particles only. For the small particles, the behavior is qualitatively the same.

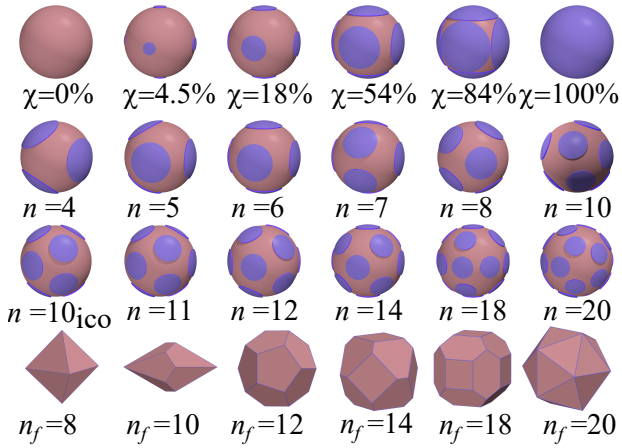

Fig. 1 Illustration of the simulation model. The top row shows particles with 6 attractive patches with varying patch sizes determined by the opening angle θ that corresponds to a certain surface coverage χ. The intermediate rows shows the patch geometry for selected numbers of patches. The patch placements correspond to the positions that maximize the minimum distance between two patches. Note that the 10_{ico}, 11, and 12-patch geometries correspond to icosahedra with two, one, and zero vertices missing. The bottom row shows the six polyhedral particles shapes, where n_f corresponds to the number of facets.

Polyhedral particle Simulations

For the polyhedral particles, we again employ EDMD simulations, predicting collisions using the separating axis theorem[46,47]. We simulate binary mixtures (composition $x = 0.5$) of polyhedral particles of identical shapes but a size ratio of 0.833. With the exception of the octahedron (8 facets), each shape with n_f facets is constructed in analogy to an n-patch particle, by drawing n planes with normals pointing along the associated patch directions at equal distance from the origin. For computational reasons, we restrict ourselves to shapes which are point-symmetric with respect to the origin. All simulated systems contained $N = 700$ particles, and were equilibrated for at least 10^5 simulation time units $\tau = \sqrt{m\sigma_L^2/k_BT}$, with the length scale σ chosen such that the volume of a large particle equals σ_L^3. Pressures were calculated from collisions using the virial theorem.

2.3 Analysis

To explore dynamics, we measure the dimensionless diffusion coefficient $D\tau/\sigma_L^2$, which is related to the mean square

View Article Online
DOI: 10.1039/C9SM01746A

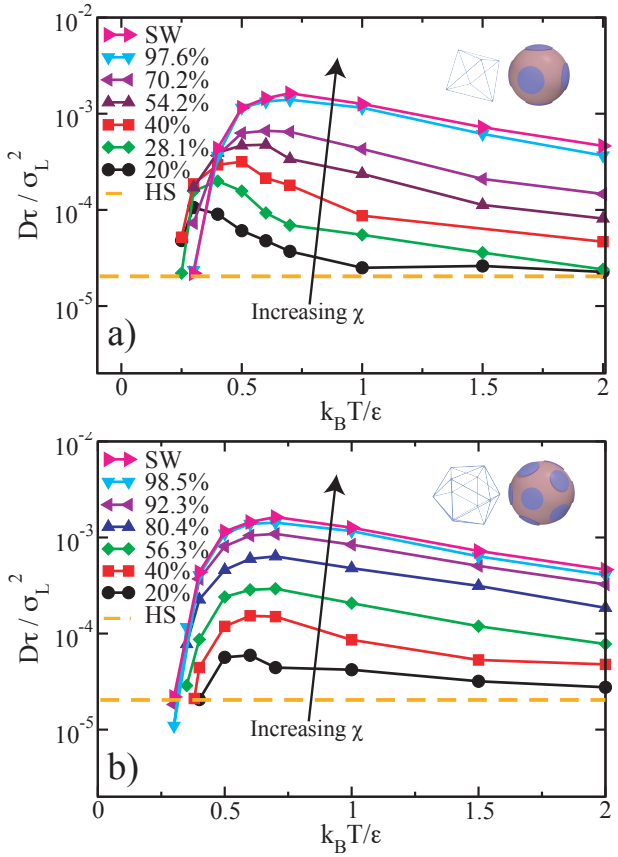

Fig. 2 Translational diffusion coefficient calculated for a system of 6 patches (**a**) and 12 patches (**b**). Dashed lines correspond to the HS limit and the right triangles to the SW limit.

displacement by Einstein diffusion equation as: $D\tau/\sigma_L^2 = \lim_{t\to\infty} \frac{1}{6N\tau} \left\langle \sum_{j=1}^{N} \left[r_j(\tau) - r_j(0) \right]^2 \right\rangle$, where N is the number of particles. We fit a linear function to the mean square displacement and obtain the diffusion coefficient with the previous expression.

In order to quantify the relaxation of the systems, we measure the time-dependent intermediate scattering function:

$$F(q,t) = \frac{\langle \rho(-\mathbf{q},t)\rho(\mathbf{q},0)\rangle}{\langle \rho(-\mathbf{q},0)\rho(\mathbf{q},0)\rangle}, \qquad (1)$$

where $\rho(\mathbf{q},t)$ is the Fourier transform of the density. From $F(q,t)$, we extract the relaxation time $\tau_{0.3}$ by fitting it with a stretched exponential: $\alpha \exp[-(\beta t)^\gamma]$, where α, β and γ are constants. The relaxation time $\tau_{0.3}$ is the time where the correlation decays to 0.3.

3 Results

3.1 Reentrant behavior

We begin our analysis by investigating whether the reentrant behavior of the diffusion coefficient as a function of temperature persists in the presence of directional interactions. To this end, we measure the dimensionless diffusion coefficient $D\tau/\sigma_L^2$, where τ and σ_L are the units of time and length respectively. In Fig. 2a, we show this diffusion coefficient for systems with $n = 6$ patches, as a function of the reduced temperature k_BT/ε, for a number of different values of the patch coverage fraction χ. In the limit of high χ, we recover the case of an isotropic square-well model in the supercooled regime, and find reentrant diffusive behavior[22,48], where the system crosses over from an attractive glass to a repulsive one. In the present work, we will use the term *attractive glass* to name the arrested state at low temperature. The fact that this phase may be a continuation of the gel phase at low density[49] is not a fundamental distinction for our results.

Upon decreasing χ, we observe an overall decrease in the diffusion, as shown in Fig. 2a, which retains its reentrant behavior as observed in a recent mean-field solution for a simpler patch geometry[50]. However, the maximum in the diffusion rate shifts to lower temperatures as χ decreases. This behavior can be understood from the observation that particles with lower coverage fractions form fewer bonds, implying that lower temperatures are required before bonding can similarly affect the dynamics. In the case of 12-patch particles (Fig. 2b) we see a similar decrease in diffusivity by decreasing patch size, but the shift in the maximum is less pronounced. We observe similar trends for the other patch geometries we explored.

3.2 Same coverage

In order to explore the effect of the patch geometry in more detail, from now on we compare systems only at the same coverage fraction $\chi = 40\%$. In Fig. 3a we plot the diffusion constant as a function of the patch geometry for different temperatures. Surprisingly, we see that the diffusion coefficient is largely independent of the patch geometry, except when the patch geometry matches icosahedral order (i.e. 10_{ico}, 11 or 12 patches). In the latter case, we instead see an extreme slowdown of the system at low temperature. Note that for several patch geometries (13, 14, 18, and 20-patch), we observe crystallization at the lowest temperatures investigated, as will be discussed later on. These points have been omitted from Fig. 3a. In the inset of Fig. 3a we show the behavior of the two geometries of the 10-patches. The icosahedral placement ($n = 10_{ico}$) presents slower dynamics at low temperatures when compared to the 10-patch geometry obtained from the spherical code ($n = 10$). In the following, we will show only the results of the 10_{ico} geometry, as the other 10-patch geometry essentially follows the trend of all other non-icosahedral patch placements.

To make a more complete analysis of the dynamics, we measure in each system the intermediate scattering function $F(q,t)$, which characterizes the relaxation time in the system at different length scales specified by the wave vector q. In Fig. 3b, we plot these correlation functions for temperature $k_BT/\varepsilon = 0.4$, at the value of q corresponding to the first peak in the structure factor (see SI). We observe an approximate collapse of the correlation functions for most geometries, while the 10_{ico}, 11, and 12-patch systems are clear outliers which relax much more slowly. We define the relaxation time $\tau_{0.3}$ as the time at which the correlation function decays to 0.3. We show in the inset of Fig. 3b the behavior of $\tau_{0.3}$ as a function of the number of patches, where the 10_{ico}, 11, and 12-patch cases show larger relaxation times. To confirm that the collapse of correlation functions is independent of q, we plot

View Article Online
DOI: 10.1039/C9SM01746A

in Fig. 3c the relaxation times as a function of q. Clearly, most systems relax at approximately the same rate, regardless of the length scale. However, the relaxation dynamics of the 10_{ico}, 11, and 12-patch particles are much slower, with the 12-patch system being roughly two orders of magnitude slower. Note that the relaxation time is significantly more affected by icosahedral patch placement than the diffusion time, which only varies by about one order of magnitude at the same temperature (red line in Fig. 3a. This suggests a strong breakdown of the Stokes-Einstein relation. This is a common feature in glassy supercooled liquids, and has been linked to the emergence of local structure[51].

The exceptionally slow dynamics of the 12-patch system correlate with a significantly larger degree of bonding in the system. In Fig. 4a, we plot the number of bond N_b per particle as a function of temperature for the different patch geometries, as well as the square-well system. As expected, in the patchy systems, bond formation is more restrictive than in the square-well system and hence lower temperatures are required to form an equivalent number of bonds. This is consistent with the overall shift to lower k_BT of the dynamical features seen in Fig. 2b for low coverage fractions. The shapes of the curves are similar and it is indeed possible to obtain a master curve, presented in the inset of Fig. 4a, once the temperature is rescaled by the temperature $T(N_b = 2)$ at which 2 bonds per particle are attained. This suggests that the number of bonds scales trivially with an activation temperature for all geometries. Interestingly, the same collapse does not occur for the diffusivity presented in Fig. 4b. The diffusivity is slowest in the 12-patch system even when comparing systems with the same number of bonds per particle.

3.3 Local Structure

To explore cage structure in more detail, we now focus on the local ordering in the fluid. To this end, we analyze the prevalence of different local structural motifs in our systems using the Topological Cluster Classification (TCC) approach[52]. This method detects local clusters of particles in a configuration, based on the connectivity of the Voronoi construction. In particular, we look for TCC motifs matching either icosahedral order (13A) or crystalline order (face-centered cubic (FCC), hexagonal close-packing (HCP), or the 9X cluster matching body-centered cubic (BCC)) (see SI). We additionally check for the formation of crystal structures belonging to the Laves phases ($MgZn_2$, $MgCu_2$, and $MgNi_2$), which are known to be stable in binary hard-sphere mixtures near this size ratio[53]. To this end, we identify local icosahedral environments matching these crystals. Specifically, there are two local environments in the Laves phases with an icosahedral topology, both with a small particle in the center. Hence, to identify the local "Laves-like" clusters, we count all icosahedral clusters with a small particle at the center, and an arrangement of large and small particles in the surrounding shell which matches one of these two environments.

In Fig. 5a, we show the fraction of particles that are part of at least one cluster of each type, for a fixed temperature $k_BT/\varepsilon = 0.4$ and for all patch geometries. As expected, for systems where crystallization occurred (14-patch and 18-patch), we see large peaks

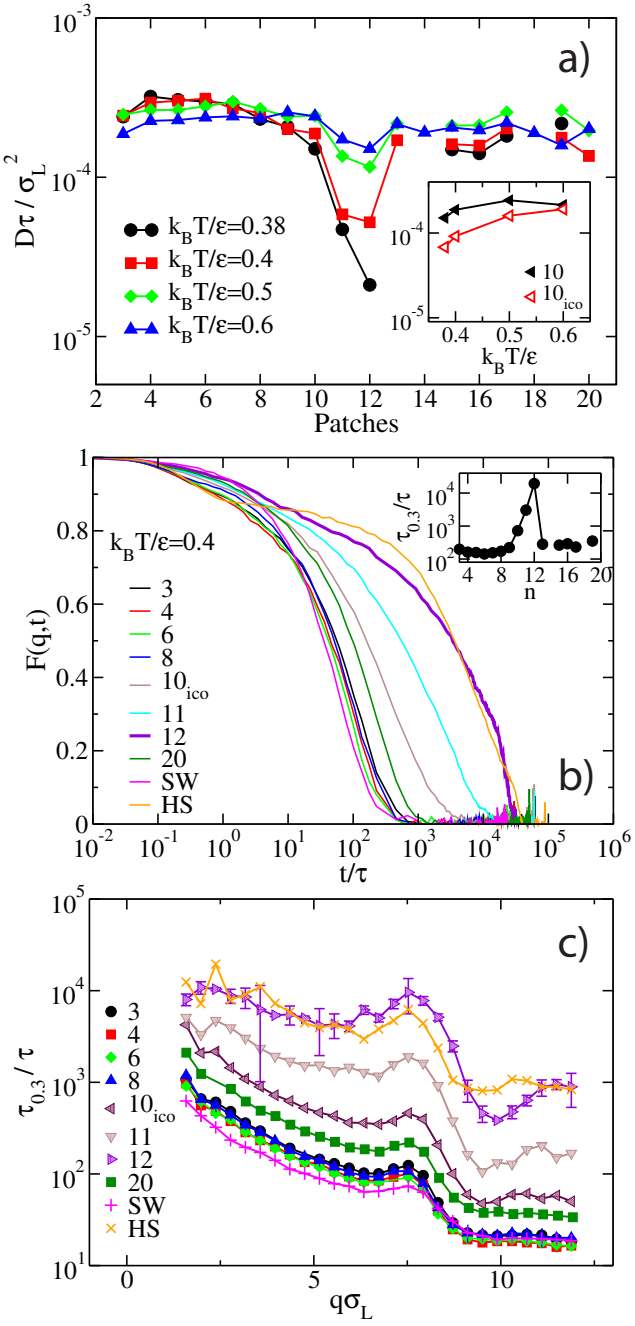

Fig. 3 a) Diffusion coefficient as a function of number of patches, at different temperatures, for patchy particles with a fixed overall patch coverage fraction $\chi = 40\%$. Missing points correspond to crystallized systems. The inset shows the diffusion coefficient as function of temperature for the $n = 10$ and $n = 10_{ico}$ cases. **b)** Intermediate scattering function of the same systems, for a wavevector q corresponding to the first peak of the structure factor, at fixed temperature $k_BT/\varepsilon = 0.4$. The inset shows the relaxation time $\tau_0.3$ as a function of the number of patches. **c)** Wave vector dependence of the relaxation time $\tau_{0.3}$, at the same temperature.

View Article Online
DOI: 10.1039/C9SM01746A

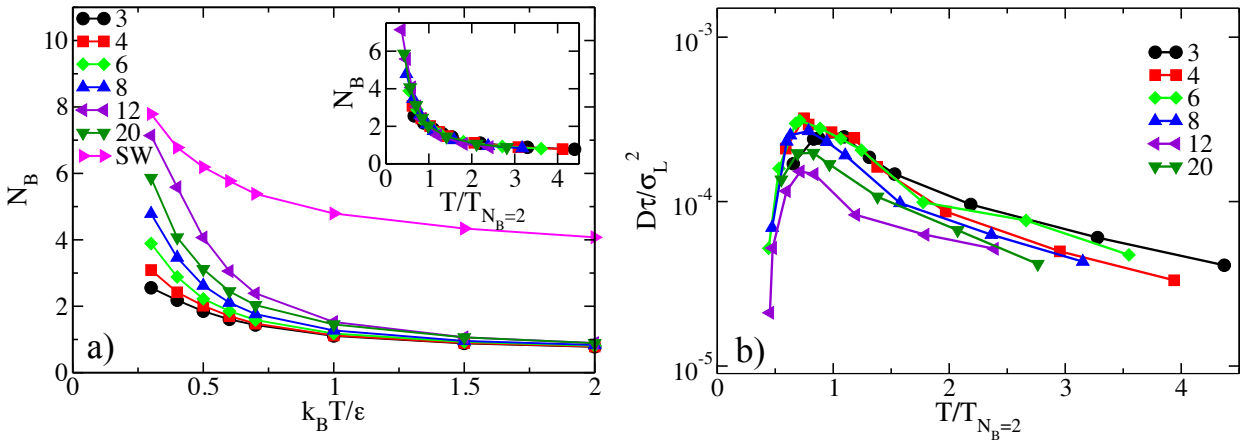

Fig. 4 a) Number of bonds per particle as a function of temperature for different patch geometries, with $\chi = 40\%$. SW indicates the square-well system. Inset plot shows the number of bonds per particle with rescaled temperature $T/T(N_b = 2)$. For each patch geometry, the temperature is normalized with the temperature at which the system forms an average of two bonds per particle. b) Diffusion coefficient as a function of rescaled temperature for different patch geometries.

in the populations of "crystal-like" clusters (FCC, BCC, HCP). In contrast, the other systems show little crystallinity, with the exception of the BCC motif, which is present in all fluids and does not indicate crystallinity on its own[52]. Icosahedral order is only observed in significant amounts for the 10_{ico}, 11, and 12-patch systems (which all match icosahedral symmetry), with the 12-patch system showing the largest fraction of icosahedral motifs. The relaxation time, shown in the same figure, follows the same trend as the number of particles involved in icosahedral clusters. These systems also display a strong drop in BCC ordering. This can be understood from the observation that the appearance of a structural motif can inhibit the prevalence of other local structures[54], and hence assist in avoiding crystallization[55,56]. Indeed, in hard-sphere fluids, the five-fold order that is present in icosahedral clusters strongly anticorrelates with BCC ordering[56]. Note that the fraction of Laves phase clusters is negligible in all systems (i.e. a few isolated motifs of this type per configuration).

In Fig. 5b, we plot the number of icosahedral motifs as a function of temperature for different patch geometries, as well as the square-well system. In the limit of high temperatures (i.e. the hard-sphere limit), we find that a significant fraction ($\approx 12\%$) of the particles are part of an icosahedral motif. As the temperature decreases, the number of icosahedral motifs initially decreases in a similar fashion for all patch geometries. In this regime, the patches essentially act, on average, as a weaker square well, and aid in the cage-breaking that enforce the reentrant behaviour observed in Fig.2. However, at low temperatures, the 10_{ico}, 11, and 12-patch systems start to display a strong enhancement of local icosahedral order, reaching values well beyond the hard-sphere level while all other patch geometries continue to further suppress icosahedral motifs. Interestingly, at very low temperatures, the square-well system also enhances icosahedral order and does so quite suddenly, possibly hinting at a phase separation[49].

It is important to note that perfect icosahedral cages are not the only structures enhanced by 10_{ico}, 11, and 12-patch particles. Intuitively, we expect the patchy interactions to have a positive effect on the concentration of any local structure which is commensurate with the chosen patch geometry. As such, there are other local structures with imperfect icosahedral order, such as defective icosahedra (see SI), whose concentration is strongly correlated with the appearance of perfect icosahedral clusters. As many of these structures incorporate the five-fold symmetry associated with the 12-patch geometry, these additional structures are all likely to contribute to both slowing down the dynamics suppressing crystallization[6,36,57].

3.4 Crystallization

For specific patch numbers ($n = 13, 14, 18, 20$), we find crystallization at the lowest temperatures investigated ($k_BT/\varepsilon \lesssim 0.4$). Specifically, we find two distinct crystal structures: a binary CsCl crystal, and a FCC crystal consisting of large particles. The CsCl structure, which consists of two interspersed simple cubic lattices, only appears in the system with $n = 20$ patches. In this structure, each particle has eight nearest neighbors of the opposite species, arranged on the vertices of a cube. The emergence of this crystal structure can be understood from the fact that the 20 patches are arranged on the vertices of a dodecahedron. This arrangement contains subsets of 8 patches that are arranged perfectly on the vertices of a cube, and hence this patch arrangement is highly compatible with the CsCl structure. We only observe the formation of FCC crystals at low temperatures for a few patch geometries ($n = 13, 14, 18$), all corresponding to a relatively large number of patches. This structure is stable in the hard-sphere limit, and is evidently further promoted by the interactions corresponding to these patch geometries. In contrast, for other patch geometries, simulations starting from an initial configuration containing a large FCC cluster consistently melt back into the fluid. From this, we conclude that for most patch geometries, crystallization into the FCC structure is disfavored in the investigated regime.

View Article Online
DOI: 10.1039/C9SM01746A

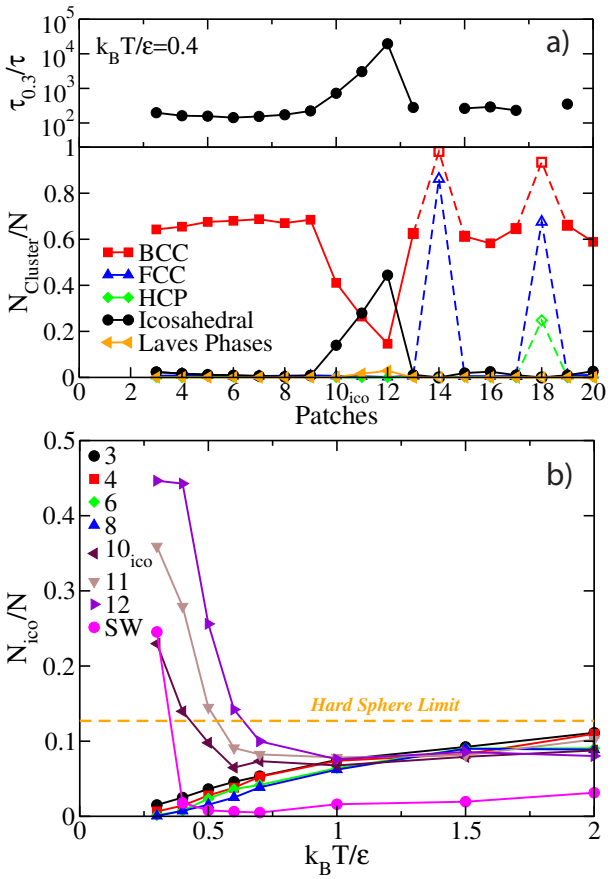

Fig. 5 Fraction of particles that are part of local structural motifs with specific symmetries, as obtained using Topological Cluster Classification[52]. **a)** Different structural motifs at a fixed temperature $k_B T/\varepsilon = 0.4$. The top panel in **(a)** shows the corresponding relaxation time $\tau_{0.3}/\tau$. Note that the systems with 14 and 18 patches have partially crystallized into an FCC structure. **b)** Particles in icosahedral clusters as a function of temperature for different patch numbers. The dashed horizontal line indicates the value in the hard-sphere limit.

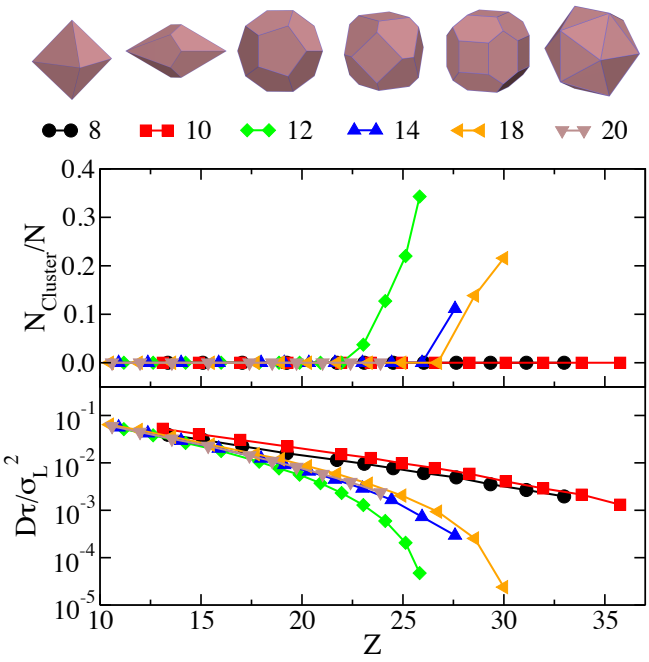

Fig. 6 **a)** Illustrations of the six polyhedral particles shapes. Note that for $n_f = 10, 12, 14, 18$, and 20, the facets are oriented in the same direction as the patches on the corresponding patchy particles. For $n_f = 8$, the shape is a perfect octahedron. **b)** Fraction of polyhedral particles that are part of an icosahedral cluster, as a function of the reduced pressure Z. We consider six shapes with different numbers of facets as indicated, corresponding to the images in Fig. 1. **c)** Diffusion coefficient D as a function of the compressibility Z. Only data for systems that remain in the fluid phase is shown. We observe crystallization upon further compression for all shapes except the 12-facet and 18-facet ones.

3.5 A purely repulsive analogue

Finally, we want to demonstrate that the correlation between the local structure and the dynamics of the systems, discussed so far, is not restricted to attraction-driven arrest. Up to this point, we have focused on the dynamics in the low-temperature regime, where we approach the attractive glass state. In the regime close to the repulsive glass (i.e. at high temperatures), the patchy interactions are too weak to significantly affect the structure of the fluid. This raises the question whether the dynamics of *repulsive* glasses can similarly be slowed down by enhancing local icosahedral order.

To test this, we explore the family of polyhedral particles shown in the top row of Fig. 6. We focus on six shapes, each with a different number of faces which will function as "entropic patches"[39]. As the system is compressed, these particles are expected to maximize their free volume (and hence entropy) by aligning face-to-face, leading to an effective attractive interaction between the facets. Due to the absence of any energetic interactions, the approach to the glass transition in hard-particle systems is controlled by the reduced pressure $Z = P/\rho k_B T$ (with P the pressure and ρ the number density) rather than the temperature[58].

Hence, in Fig. 6b, we plot the number of particles found in icosahedral environments as a function of Z for all six shapes. Additionally, in Fig. 6c, we show the associated diffusion coefficients. We find that, in perfect analogy to the patchy-particle systems, the 12-facet particles (dodecahedra) strongly promote local icosahedral order, leading to much slower dynamics. Moreover, the other particle shapes show less or no icosahedral ordering, and require significantly stronger compression before dynamical slowdown occurs. Hence, the direct link between icosahedral ordering and slow dynamics is maintained even in this inherently different class of glassy fluids.

4 Conclusion

Icosahedral local order has been linked to both dynamical slowdown[59–61], and to the suppression of crystallization[36,40–42], making it an ideal tool for the design of glassy materials. Here, we demonstrated that dynamical slowdown can be enhanced by designing particle interactions which match and reinforce the long-lived local icosahedral structure responsible for caging in the repulsive glass[61,62]. In contrast, for the 15 other patch geometries we explored, which do not match local icosahedral order, the patch placement has surprisingly little impact on the dynamics of

View Article Online
DOI: 10.1039/C9SM01746A

the system. Hence, our results suggest that – for the spherical and polyhedral particles studied here – icosahedral motifs are unique in their ability to slow down dynamics. This extreme sensitivity of dynamics to local icosahedral structures highlights the important role these motifs play in the kinetic arrest of disordered systems. Moreover, the inherent incompatibility of icosahedral order with long-ranged crystalline order suggests that these systems are also virtually guaranteed to avoid crystallization.

Our results demonstrate that we can control the dynamical slowdown of supercooled liquids by designing particles that inherently promote or disrupt the formation of "slow" local environments. Here, we used binary mixtures of hard-core particles as a starting point, and found that the local structures which are most effective at slowing down the system are icosahedral in nature. However, it is easy to imagine systems where icosahedral order is inherently disfavored by the interactions of the particle cores. Strongly anistropic (e.g. rod-like) particles, or particles with soft-core interactions often inherently favor a number of neighbors that is different from 12. In these situations, a different local configuration may take over the role of the "slow" structural motif, and enhancing local icosahedral order will likely have little effect on the local dynamics[60,63]. However, for the broad class of particles which are roughly spherical, our results demonstrate that engineering the local structure of fluids provides an extremely promising route towards controlling their dynamics.

Conflicts of interest

There are no conflicts to declare.

Acknowledgements

We thank Francesco Sciortino and Paddy Royall for useful discussions. S. Marín-Aguilar acknowledges CONACyT for funding.

Notes and references

1 L. Berthier and G. Biroli, *Rev. Mod. Phys.*, 2011, **83**, 587–645.
2 G. L. Hunter and E. R. Weeks, *Rep. Prog. Phys.*, 2012, **75**, 066501.
3 H. Tanaka, H. Tong, R. Shi and J. Russo, *Nature Reviews Physics*, 2019, 1.
4 G. Tarjus, S. A. Kivelson, Z. Nussinov and P. Viot, *J. Phys.: Condens. Matter*, 2005, **17**, R1143.
5 J. E. Hallet, F. Turci and P. Royall, *Nat. Commun.*, 2018, **9**, 3272.
6 A. Malins, J. Eggers, C. P. Royall, S. R. Williams and H. Tanaka, *J. Chem. Phys.*, 2013, **138**, 12A535.
7 C. P. Royall and S. R. Williams, *Phys. Rep.*, 2015, **560**, 1–75.
8 C. P. Royall and W. Kob, *J. Stat. Mech.: Theo. Exp.*, 2017, **2017**, 024001.
9 H. Shintani and H. Tanaka, *Nat. Phys.*, 2006, **2**, 200.
10 H. Tanaka, *J. Phys. Condens. Matter*, 2003, **15**, L491.
11 D. B. Miracle, T. Egami, K. M. Flores and K. F. Kelton, *MRS Bull.*, 2007, **32**, 629–634.
12 J. P. Doye, D. J. Wales, F. H. Zetterling and M. Dzugutov, *J. Chem. Phys.*, 2003, **118**, 2792–2799.
13 G. M. Hocky, D. Coslovich, A. Ikeda and D. R. Reichman, *Physical review letters*, 2014, **113**, 157801.
14 E. R. Weeks, J. C. Crocker, A. C. Levitt, A. Schofield and D. A. Weitz, *Science*, 2000, **287**, 627–631.
15 L. Berthier, G. Biroli, J.-P. Bouchaud, L. Cipelletti, D. E. Masri, D. L'Hôte, F. Ladieu and M. Pierno, *Science*, 2005, **310**, 1797–1800.
16 L. Berthier, D. Coslovich, A. Ninarello and M. Ozawa, *Phys. Rev. Lett.*, 2016, **116**, 238002.
17 K. N. Pham, A. M. Puertas, J. Bergenholtz, S. U. Egelhaaf, A. Moussaıd, P. N. Pusey, A. B. Schofield, M. E. Cates, M. Fuchs and W. C. Poon, *Science*, 2002, **296**, 104–106.
18 G. Foffi, K. A. Dawson, S. V. Buldyrev, F. Sciortino, E. Zaccarelli and P. Tartaglia, *Phys. Rev. E*, 2002, **65**, 050802.
19 J. Bergenholtz and M. Fuchs, *Phys. Rev. E*, 1999, **59**, 5706.
20 K. Dawson, G. Foffi, M. Fuchs, W. Götze, F. Sciortino, M. Sperl, P. Tartaglia, T. Voigtmann and E. Zaccarelli, *Phys. Rev. E*, 2000, **63**, 011401.
21 A. M. Puertas, M. Fuchs and M. E. Cates, *Phys. Rev. Lett.*, 2002, **88**, 098301.
22 E. Zaccarelli, G. Foffi, K. A. Dawson, S. V. Buldyrev, F. Sciortino and P. Tartaglia, *Phys. Rev. E*, 2002, **66**, 041402.
23 T. Eckert and E. Bartsch, *Phys. Rev. Lett.*, 2002, **89**, 125701.
24 K. N. Pham, S. U. Egelhaaf, P. N. Pusey and W. C. K. Poon, *Phys. Rev. E*, 2004, **69**, 011503.
25 R. M. Choueiri, E. Galati, H. Thérien-Aubin, A. Klinkova, E. M. Larin, A. Querejeta-Fernández, L. Han, H. L. Xin, O. Gang, E. B. Zhulina *et al.*, *Nature*, 2016, **538**, 79.
26 G.-R. Yi, D. J. Pine and S. Sacanna, *J. Phys.: Condens. Matter*, 2013, **25**, 193101.
27 V. Meester, R. W. Verweij, C. van der Wel and D. J. Kraft, *ACS Nano*, 2016, **10**, 4322–4329.
28 S. Biffi, R. Cerbino, G. Nava, F. Bomboi, F. Sciortino and T. Bellini, *Soft Matter*, 2015, **11**, 3132–3138.
29 I. I. Smalyukh, *Annu. Rev. Condens. Matter Phys.*, 2018, **9**, 207–226.
30 S. C. Glotzer and M. J. Solomon, *Nat. Mater.*, 2007, **6**, 557.
31 E. Bianchi, R. Blaak and C. N. Likos, *Phys. Chem. Chem. Phys.*, 2011, **13**, 6397.
32 W. Liu, M. Tagawa, H. L. Xin, T. Wang, H. Emamy, H. Li, K. G. Yager, F. W. Starr, A. V. Tkachenko and O. Gang, *Science*, 2016, **351**, 582–586.
33 Q. Chen, S. C. Bae and S. Granick, *Nature*, 2011, **469**, 381.
34 F. Smallenburg and F. Sciortino, *Nat. Phys.*, 2013, **9**, 554.
35 C. De Michele, S. Gabrielli, P. Tartaglia and F. Sciortino, *J. Phys. Chem. B*, 2006, **110**, 8064–8079.
36 J. Taffs and C. P. Royall, *Nat. Commun.*, 2016, **7**, 13225.
37 V. Molinero, S. Sastry and C. A. Angell, *Phys. Rev. Lett.*, 2006, **97**, 075701.
38 R. Di Leonardo, L. Angelani, G. Parisi and G. Ruocco, *Phys. Rev. Lett.*, 2000, **84**, 6054.
39 G. van Anders, N. K. Ahmed, R. Smith, M. Engel and S. C. Glotzer, *Acs Nano*, 2013, **8**, 931–940.
40 J. D. Bernal, *Nature*, 1959, **183**, 141.

View Article Online
DOI: 10.1039/C9SM01746A

41 F. C. Frank, *Proc. R. Soc. Lond. A*, 1952, **215**, 43–46.
42 N. C. Karayiannis, R. Malshe, J. J. de Pablo and M. Laso, *Phys. Rev. E*, 2011, **83**, 061505.
43 N. Kern and D. Frenkel, *J. Chem. Phys.*, 2003, **118**, 9882 – 9889.
44 N. J. A. Sloane, R. H. Hardin, W. D. Smith *et al.*, *Available at http://neilsloane.com/packings/*, 2000.
45 L. Hernández de la Peña, R. van Zon, J. Schofield and S. B. Opps, *J. Chem. Phys.*, 2007, **126**, 074105.
46 S. Gottschalk, M. C. Lin and D. Manocha, Proceedings of the 23rd annual conference on Computer graphics and interactive techniques, 1996, pp. 171–180.
47 F. Smallenburg, L. Filion, M. Marechal and M. Dijkstra, *Proceedings of the National Academy of Sciences*, 2012, **109**, 17886–17890.
48 F. Sciortino, *Nat. Mater.*, 2002, **1**, 145 – 146.
49 C. P. Royall, S. R. Williams and H. Tanaka, *J. Chem. Phys.*, 2018, **148**, 044501.
50 H. Yoshino, *arXiv preprint arXiv:1807.04095*, 2018.
51 G. Tarjus and D. Kivelson, *The Journal of chemical physics*, 1995, **103**, 3071–3073.
52 A. Malins, S. R. Williams, J. Eggers and C. P. Royall, *J. Chem. Phys.*, 2013, **139**, 234506.
53 A.-P. Hynninen, L. Filion and M. Dijkstra, *J. Chem. Phys.*, 2009, **131**, 064902.
54 P. Ronceray and P. Harrowell, *Journal of Statistical Mechanics: Theory and Experiment*, 2016, **2016**, 084002.
55 P. Ronceray and P. Harrowell, *Physical Review E*, 2017, **96**, 042602.
56 B. M. Carter, F. Turci, P. Ronceray and C. P. Royall, *The Journal of chemical physics*, 2018, **148**, 204511.
57 M. Celino, V. Rosato, A. Di Cicco, A. Trapananti and C. Massobrio, *Phys. Rev. B*, 2007, **75**, 174210.
58 L. Berthier and T. A. Witten, *Physical Review E*, 2009, **80**, 021502.
59 H. Jónsson and H. C. Andersen, *Phys. Rev. Lett.*, 1988, **60**, 2295.
60 Y. Cheng, H. Sheng and E. Ma, *Phys. Rev. B*, 2008, **78**, 014207.
61 C. P. Royall, A. Malins, A. J. Dunleavy and R. Pinney, *J. Non-Cryst. Solids*, 2015, **407**, 34–43.
62 M. Leocmach and H. Tanaka, *Nat. Commun.*, 2012, **3**, 974.
63 A. Malins, J. Eggers, H. Tanaka and C. P. Royall, *Farad. Discuss.*, 2013, **167**, 405–423.